Earthquakes and Structures, *Vol. 28, No. 5 (2025) 411-422*
https://doi.org/10.12989/eas.2025.28.5.411

Seismic design of connection between height-adjustable steel H-section column and foundation

Chaeyun Ahn[1a], Jongwon Hong[1a], Jang Keun Yoon[2b] and Thomas H.-K. Kang[*1]

[1]*Department of Architecture and Architectural Engineering, Seoul National University, 1 Gwanak-ro, Gwanak-gu, Seoul 08826, Korea*
[2]*JK E&C, 11 Uisadang-daero 1-gil, Yeongdeungpo-gu, Seoul 07332, Korea*

(Received February 1, 2025, Revised February 21, 2025, Accepted February 21, 2025)

Abstract. This study proposes an H-section dry support system for water tank foundation as a structural alternative to conventional concrete wet connections, addressing limitations such as extended curing times and limited height adjustability while ensuring seismic capacity. Static lateral loading tests on strong and weak axes of H-section confirmed the system's seismic performance such as strength and ductility, with deformation concentrated at lower joints rather than the column body. Differences in axis performance were linked to varying stress distribution patterns. A 3D finite element (FE) analysis using MIDAS Gen software was conducted on rectangular water tanks under gravity, hydrostatic and design seismic loads, with all evaluated connection arrangements meeting story drift and stability criteria. The system exceeded seismic lateral force requirements for non-structural components and low-rise buildings. It further offers improved maintenance efficiency through easy component replacement and height adjustability, reducing lifecycle costs and enhancing construction efficiency.

Keywords: construction efficiency; seismic resistance; steel H-section dry connection; structural performance analysis; water tank foundation

1. Introduction

Water tank is an essential element for most buildings or regions in modern society, and the structural safety of water tanks for stable water supply is crucial (Beak *et al.* 2019, Hosseini and Beskhyroun 2023). Structural resistance to earthquakes is particularly vital for the long-term operation and maintenance of facilities. Historical seismic events have documented cases of damage to large liquid storage tanks, and such damage has been proven to lead to secondary damage such as fires (Ximei *et al.*, Fischer *et al.* 2016).

Thus, regulations worldwide present standards to ensure the safety and functionality of tanks. ASCE 7-16 (ACI 2017) classifies tanks and storage vessels not supported by buildings as non-building structures and provides a method for calculating seismic loads that considers the dynamic behavior of internal fluids (Baek and Choi 2017). The dynamic characteristics are presented in the design standards based on Housner's analytical model, which separates the impulsive and convective (i.e., sloshing) components (Housner 1957). These dynamic characteristics are reflected in various design standards. For concrete water tanks, ACI 350.3 (ACI 2006) are commonly referenced, while steel water tanks follow the D100 and D103 (AWWA 2011), providing detailed requirements for tank design. On the other hand, when tanks are installed within buildings, they are considered supported by the structure, and the dynamic behavior of the fluid is not taken into account. In Japan, where earthquakes are frequent, the FRP (Fiber Reinforced Plastic) tank structural design (JAC 2014) calculation method is used, which more specifically regulates the response amplification of both the building and the water tank (Park *et al.* 2013).

Numerous studies have been conducted on the seismic design of liquid storage tanks. However, research focusing specifically on the foundation of tanks remains insufficient (Brunesi *et al.* 2015, Cruz and Valdivia 2011, Sobhan *et al.* 2017, Stewart *et al.* 1999, Ulloa-Rojas *et al.* 2024, Yazdanian *et al.* 2020, Zareian *et al.* 2012). The foundation supporting the tank plays a critical role in transferring loads between the tank and the supporting surface, effectively distributing both static and dynamic loads to prevent structural damage, making its consideration essential in tank design. Recent studies have demonstrated that inadequate detailing of foundation anchors can lead to tank wall rupture and that if the foundation shear force exceeds the frictional force, the tank may slide (Praveen *et al.* 2000).

Traditional tank foundation systems have conventionally used concrete wet connections, which have limitations such as the need for a curing period during construction and difficulties in height adjustment (Robert 1964, Khosravi *et al.* 2023). Some base isolation devices made of rubber pads have also been used, but they lack durability and long-term performance (Kim *et al.* 2016). Among various materials, H-section steel dry connections have been evaluated to provide the best performance after installation, as their high stiffness ensures structural stability (Hou *et al.* 2021, Kong

*Corresponding author, Professor
E-mail: tkang@snu.ac.kr
[a]Master's Student
[b]P.E.

ISSN: 2092-7614 (Print), 2092-7622 (Online)

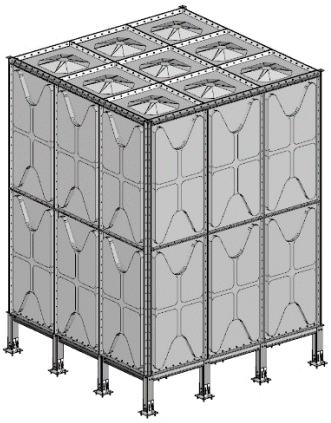

(a) Water tank

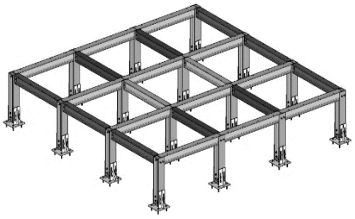

(b) Dry connections supporting water tank

Fig. 1 Isometric view

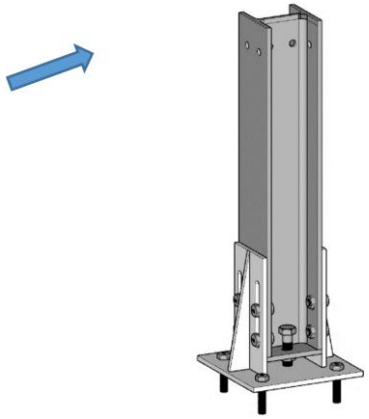

(a) Strong axis direction

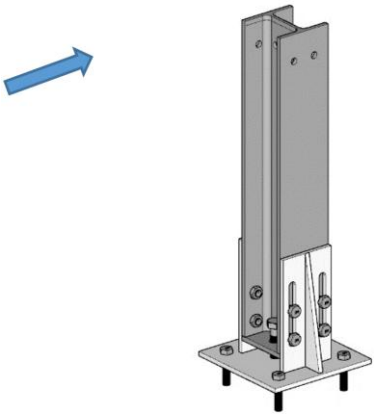

(b) Weak axis direction

Fig. 2 Three-dimensional representation and directional definition of H-section column

et al. 2024, Liu *et al.* 2019). Several researchers have indicated that the detailing of base plate connections in certain designs can be highly cost-intensive and challenging to fabricate, emphasizing the importance of establishing standardized design guidelines for such connections (Fasaee *et al.* 2018, Kanvinde *et al.* 2013, Lim *et al.* 2017, Torres-Rodas *et al.* 2018, Nechache and Bouzide 2007).

This study proposes an innovative height-adjustable bolted base connection system to overcome the limitations of conventional H-section steel dry connections. To verify the structural performance of the proposed system, unidirectional static lateral loading tests were conducted along both the strong and weak axes of H-section. The results confirmed sufficient seismic resistance and practical applicability. As will be discussed in detail in Section 4, the system effectively responds to ground settlement issues through its height-adjustable feature and ease of component replacement, which is expected to contribute to reducing the life-cycle costs of the facility (Thakur *et al.* 2017). In particular, compared to conventional wet connection systems, the proposed system demonstrated significant improvements in on-site applicability and construction efficiency while maintaining superior structural performance. Furthermore, a 3D finite element analysis was performed on a typical rectangular water tank to determine the optimal connection arrangement with regard to the strong and weak axes. This study primarily focused on static analysis, following the simplified approaches permitted by design standards, which was deemed sufficient to validate the foundational study even without considering sloshing effects. Through this experimental validation, the study presents an innovative improvement to water tank foundation systems, aiming to contribute to advancements in the non-structural component construction sector.

2. Experimental research

2.1 General

The H-section steel dry connections are characterized by being installed at 1.0 m intervals symmetrically in both principal directions at the bottom of the water tank, as shown in Figs. 1(a)-(b). All dry connection details are identical and feature an H-section steel cross-section with strong and weak axes, as illustrated in Figs. 2(a)-(b). The H-section steel columns are of H-100×100×6×8 mm (4×4×0.2×0.3 in.) specification and are connected at the flange with splice plates and high-tension bolts, resisting seismic loads transmitted to the bottom of the water tank.

The splice plates are welded to the base plate together with gusset plates. The steel material used in these components is SS275 (KS D 3503), which has a yield strength of 275 MPa (39,885 psi). The splice plate dimensions are 150×200×8 mm (6×8×0.3 in.), and a 103 mm (4 in.) long-slotted hole is provided to allow for flexible height adjustment of the H-section steel column (see Fig. 3). Additionally, the horizontal end plates welded on both sides of the H-section web are seated on top of the nut, with a bolt inserted through the hole in the horizontal plate and connected to the base plate, enabling temporary support and positional adjustment during construction.

The high-tension bolts are F8T bolts with a tensile

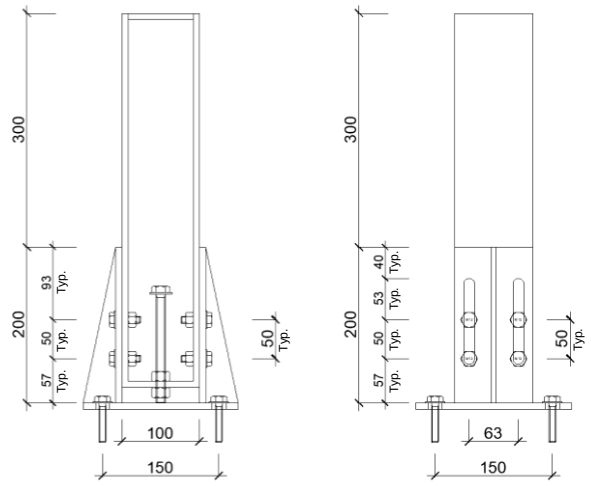

(a) Strong axis direction (b) Weak axis direction

Fig. 3 Typical details of adjustable-height steel H-section and its dry connection to foundation (Unit: mm)

strength of 800 MPa (116,030 psi). The bolts have a diameter of M12 (12 mm) with a pitch of 1.75 mm (0.07 in.). Among the bolts installed in the section, the 4 lower bolts are positioned at the bottom part of the slotted hole, located about 57 mm (2 in.) above the base plate. The 4 upper bolts are placed 50 mm (2 in.) higher, at a vertical length of 107 mm (4 in.). The bolts are mechanically tightened using a torque wrench.

In this study, unidirectional static lateral loading tests were conducted on the strong and weak axes of the H-section steel dry connections to verify their seismic performance.

2.2 Material testing

Prior to the structural testing, a material test was conducted using a total of five coupon tensile specimens to evaluate the mechanical properties of the steel used and verify whether it meets the minimum strength requirements specified in the design standards. The tensile test was performed using a Universal Testing Machine (UTM), which enabled the precise measurement of the yield strength and tensile strength of each specimen.

The tensile test was conducted by gradually applying tensile loads to the specimens while observing the material's yield and fracture behavior. During the test, the elongation and load variations of each specimen were recorded, and these data were used to determine the yield point and maximum tensile strength of the steel. This process aimed to assess the quality of the steel used and ensure that it meets the minimum performance criteria required by the design specifications.

The coupon specimens used in this test were extracted from the same lot of steel as that used in the fabrication of the dry pads and the H-beam body, ensuring the reliability and representativeness of the test results.

Tensile tests were conducted on a total of five coupon steel specimens, and the results confirmed that all specimens satisfied the minimum yield strength criteria for

Table 1 Material test results [MPa]

	C1	C2	C3	C4	C5	Average
Yield strength (F_y)	277	280	375	340	376	330
Tensile strength (F_u)	367	369	465	430	467	420

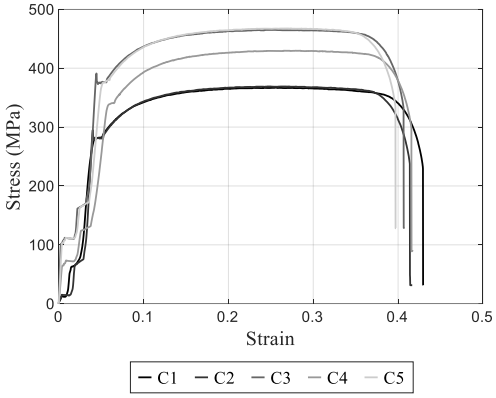

Fig. 4 Stress-strain curve of steel specimen

SS275 steel (KS D 3503). The minimum yield strength requirement for SS275 steel is specified as 275 MPa (39,885 psi), and the steel used in this test demonstrated performance that sufficiently exceeded this requirement.

Tensile tests were conducted on a total of five coupon steel specimens, and the results confirmed that all specimens satisfied the minimum yield strength criteria for SS275 steel (KS D 3503). The minimum yield strength requirement for SS275 steel is specified as 275 MPa (39,885 psi), and the steel used in this test demonstrated performance that sufficiently exceeded this requirement.

The detailed tensile test results for each coupon specimen, denoted as C1 through C5, are summarized in Table 1, with an average yield strength measured at 330 MPa (47,863 psi) and an average tensile strength of 420 MPa (60,916 psi). The individual yield strengths ranged from 277 MPa (40,176 psi) to 376 MPa (54,534 psi), while the tensile strengths ranged from 367 MPa (53,229 psi) to 467 MPa (67,733 psi), indicating excellent consistency and quality of the steel.

Fig. 4 presents the graphical representation of the tensile test results. This result confirms the superior mechanical performance of the steel, making it suitable for use in structural testing.

Furthermore, the elongation of all specimens also met the minimum requirements, and the reduction in the cross-sectional area after fracture was confirmed to exceed the minimum criteria. These findings suggest that the steel possesses sufficient ductility.

The material test validated that the SS275 steel used meets the strength and elongation KS requirements necessary for structural testing, providing reliable baseline data to support the subsequent structural experiments.

2.3 Structural testing

The tests were performed on six dry column-to-

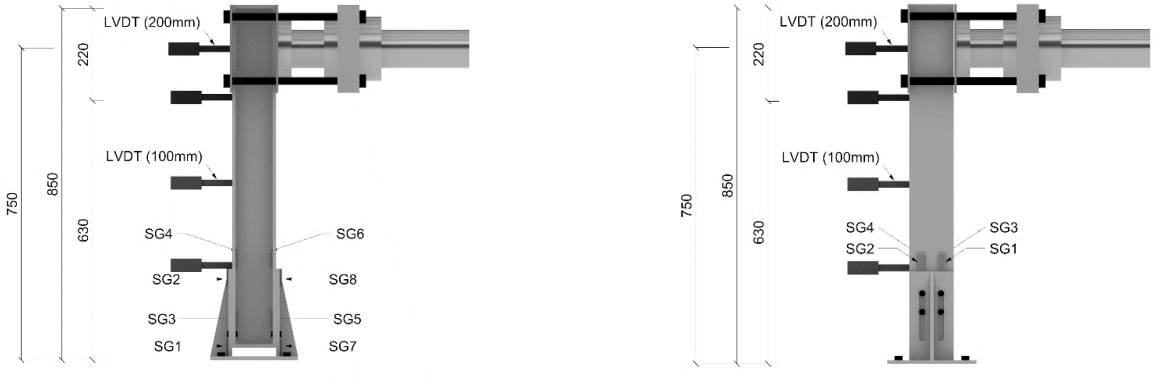

(a) Strong axis direction specimen (b) Weak axis direction specimen

Fig. 5 Actuator load plan (mm)

Table 2 Structural testing

Testing type	Uniaxial static lateral load test
Testing equinpment	15 Ton actuator
Loading speed	0.005 mm/sec (Displacement-controlled)
Specimen height	850 mm
Loading height	750 mm
Experimental variables	Loading Direction (Strong axis, Weak axis)
Number of specimens	Strong axis (3), Weak axis (3)
LVDT	200 mm (2 units), 100 mm (2 units)
Strain gauge	Strong axis (8 units), Weak axis (4 units)

foundation connection specimens. A 150 kN (34 kips) actuator was used, and the tests were displacement-controlled. The specimen height was adjusted to 850 mm (33 in.) to secure the loading area. The variables are the loading directions (x direction and y direction, which are also referred to as the strong axis and weak axis of H-section, respectively). The layout of linear variable displacement transducers (LVDTs) for displacement measurement and strain gauges (SG) for strain measurement is shown in Fig. 5, and the directional static lateral force test overview is summarized in Table 2.

The base plate of the specimens was fixed to achieve fixed support conditions using bolt anchors commonly utilized in the testing facility. The actuator load application height was set at 750 mm (30 in.). Protective steel plates measuring 200×200×5 mm (8×8×0.2 in.) were installed at the upper loading points for fixation. For all specimens, lateral load and displacement were measured using the actuator's built-in system and LVDTs, respectively. A total of four LVDTs were installed at positions of 200 mm (8 in.), 415 mm (16 in.), 630 mm (25 in.), and 750 mm (30 in.) from the ground to measure the displacement of the bending specimen. Among them, the two upper LVDTs, where greater displacement was expected, were devices capable of measuring up to 200 mm (8 in.), while the lower ones were devices capable of measuring up to 100 mm (4 in.). The load-displacement curves were derived to evaluate seismic performance

Additionally, the strong axis test used regular 4 bolts (no high-tension bolts) to connect the splice plate and H-section; however, after the strong axis test, it was realized that the moment resistance mechanism was not found only using 4 bolts at the bottom part so that a total of 8 high-tension bolts (2 for each long-slotted hole) were used for the weak axis test.

2.4 Experimental results

2.4.1 Failure patterns and load-displacement relationships

The tests were terminated at approximately 10 kN for the strong axis and 12 kN for the weak axis to prevent specimen overturning. However, the actual ultimate tensile strength is expected to exceed the measured values.

The results of the loading tests in the strong and weak axis directions can be observed in Figs. 6 and 7, respectively. At this stage, following the sequence of the experiment, the specimens loaded in the strong axis direction were designated as S1 through S3, while those loaded in the weak axis direction were designated as W1 through W3. All six specimens were fabricated using the same material and dimensions, ensuring homogeneity for obtaining average experimental values. As shown in Fig. 8(a), which illustrates the load-displacement relationship obtained from the LVDT measurements, for the strong axis loading test, S1 and S3 exhibited sequential bolt slippage, leading to a lower initial strength but higher yield strength compared to S2, which experienced simultaneous slippage.

(a) S1 - At maximum displacement (b) S1 - At bottom failure

(c) S2 - At maximum displacement (d) S2 - At bottom failure

(e) S3 - At maximum displacement (f) S3 - At bottom failure

Fig. 6 Strong axis direction test results

Conversely, as depicted in Fig. 8(b), for the weak axis loading test, W1 and W3 with sequential bolt slippage showed both lower initial and yield strength than W2, indicating contrasting results.

These differences are primarily attributed to variations in stress distribution based on the loading direction. During strong axis loading, stress was relatively evenly distributed among the bolts, and sequential bolt slippage contributed to overall joint strength improvement through stress redistribution. On the other hand, weak axis loading induced local stress concentration at the lower joint, negating the positive effects of sequential slippage.

Ultimately, all specimens exhibited similar plastic behavior after yielding of the side splice plates. These results underscore the need to comprehensively consider bolt slippage mechanisms, localized stress concentrations, and stiffness when designing joints subjected to weak axis loads.

2.4.2 Strength assessment of the specimens

The joint strength of the steel dry connection specimens was evaluated based on the Korean Design Standard[34-38] for load and resistance factor design of steel structures.

High-tension bolt connections can be categorized into friction connections, tension connections and bearing connections. In this study, joint strength for the strong and weak axes of the H-section steel dry connections was assessed. Experimental results confirmed that both directions resisted actuator loads up to a maximum strength of 10 kN.

The design load for structural review was determined as 10 kN of horizontal shear force, which corresponds to 3.5 kN-m of bending moment. The specifications of the high-tension bolts and steel materials are summarized in Tables

(a) S1 - At maximum displacement

(b) S1 - At bottom failure

(c) S2 - At maximum displacement

(d) S2 - At bottom failure

(e) S3 - At maximum displacement

(f) S3 - At bottom failure

Fig. 7 Weak axis direction test results

3-4, respectively.

The tensile strength of the high-tension bolts in the strong axis direction was first evaluated. Using Eq. (1), the maximum shear force ($V_{u,max}$) was divided by the number of bolts (2 per splice plate were used) to calculate the maximum tensile force (P_u). The tensile resistance of the two (or four for final design) high-tension bolts on one side of the flange was calculated using Eq. (2) and found to exceed the maximum force by far (10 times).

$$P_u = \frac{V_{u,max}}{2} \tag{1}$$

$$\phi R_n = \phi \times F_{nt} \times A_b \tag{2}$$

Where, P_u is the maximum tensile force per bolt, obtained by dividing the total shear force by the number of bolts, N or lb; $V_{u,max}$ is the maximum shear force induced by seismic loads, N or lb; ϕ is a factor applied to tensile force (=0.75); R_n is the design strength of the slip-critical connection, N or lb; F_{nt} is the nominal tensile strength of high-tension bolts, such as F8T bolts, MPa or psi; and A_b is the nominal cross-sectional area of the unthreaded portion of a bolt or threaded rod, mm^2 or in^2.

Next, the out-of-plane bending strength of a splice plate was reviewed. The splice plate bending moment at the interface between the splice plate and base plate was determined using Eq. (3), and the plastic moment capacity of the splice plate (with no contribution of the gusset plate) was calculated using Eq. (4). The key point here is that unlike the weak axis behavior, in the strong axis behavior, the high-tension bolts do not resist shear force or bending moment. Instead, the seismic load is entirely resisted by one of the two splice plate (like a cantilever). The splice plate's out-of-plane bending performance (M_u) and the

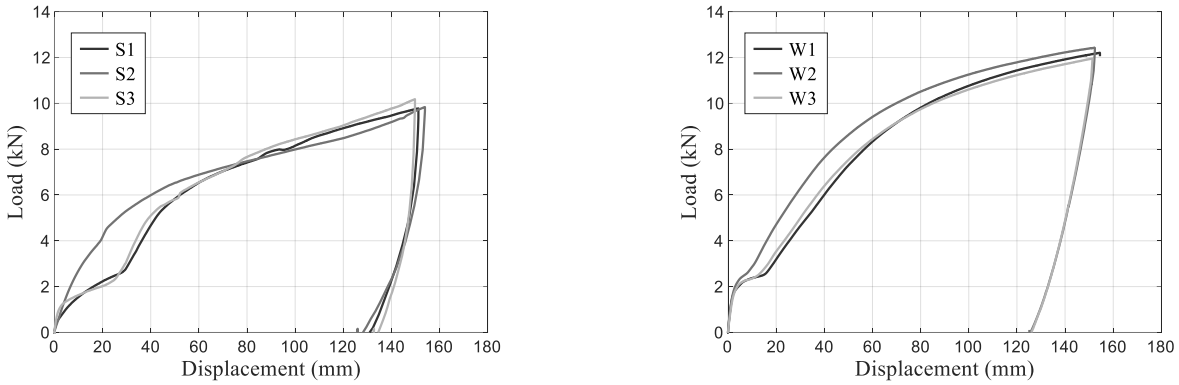

(a) Strong axis direction (b) Weak axis direction

Fig. 8 Load-displacement curve

Table 3 Specifications of high-tension bolts

F8T tensile strength (F_u)	800 MPa
F8T nominal tensile strength (F_{nt})	600 MPa
F8T nominal shear strength (F_{nv})	400 MPa
Bolt diameter (D)	12 mm
Bolt pitch (P)	1.75 mm
Nominal cross-sectional area (A_b)	113 mm^2
Effective cross-sectional area (D)	84.3 mm^2

Table 4 Specifications of steel

SS275 yield strength (F_y)	275 MPa
SS275 tensile strength (F_u)	410 MPa
Connection plate thickness (t)	8 mm
Section modulus of connection plate (Z)	10,667 mm^3

comprehensive mechanism are shown in Fig. 9(a).

$$M_{u,\max} = V_{u,\max} \times l \tag{3}$$

$$\phi M_n = \phi \times Z \times F_y \tag{4}$$

Where, $M_{u,max}$ is the maximum bending moment at the bottom of the splice plate, N-mm or lb-in; l is the cantilever height of the splice plate (conservatively assuming the lateral load is transferred to the tip of the splice plate), mm or in; ϕ is a factor applied to bending strength (=0.9); M_n is the nominal plastic moment at the bottom of the splice plate, N-mm or lb-in; Z is the plastic modulus of the splice plate, mm^3 or in^3; and F_y is the yield strength of steel, MPa or psi.

The shear strength of high-tension bolts in the weak axis direction was also evaluated. The shear force on each bolt was determined using Eq. (5) (See Fig. 9(b)). The resistance of one of four high-tension bolts was calculated using Eq. (6) and deemed sufficient to resist the maximum frictional force.

$$R_u = \frac{M_{u,max}}{a} \tag{5}$$

$$\phi R_n = \phi \times F_{nv} \times A_e \tag{6}$$

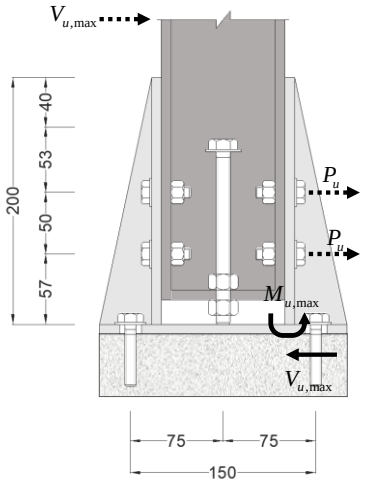

(a) Strong axis direction

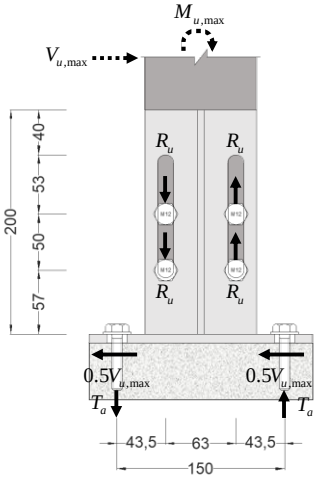

(b) Weak axis direction

Fig. 9 Load-resistance mechanism

Where, R_u is the shear force acting on a single bolt, also representing the maximum frictional force, N or lb; a is the spacing between bolts, mm or in; F_{nv} is the nominal shear strength of high-tension bolts, such as F8T bolts, MPa or psi; ϕ=0.75; and A_e is the effective cross-sectional area of the unthreaded portion of a bolt or threaded rod, mm^2 or in^2.

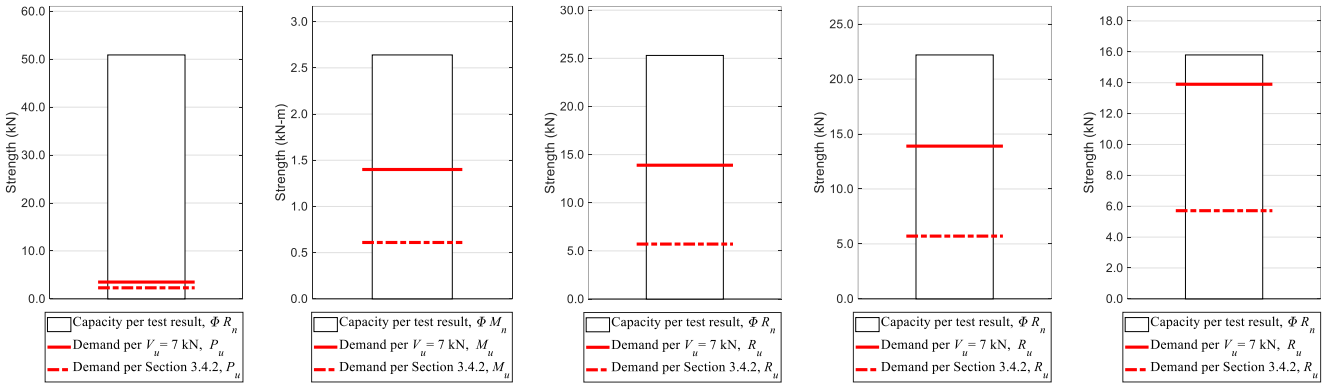

(a) Tensile strength of high-strength bolts in the strong axis direction

(b) Out-of-plane bending strength of splice plate in the strong axis direction

(c) Shear strength of high-strength bolt in the weak axis direction

(d) Bearing strength of bolt hole in the weak axis direction

(e) Slip resistance of friction-type connection in the weak axis direction

Fig. 10 Review of strength and structural safety based on experimental results (ϕ=0.75 for (a) Tensile strength; ϕ=0.9 for (b) Bending strength; ϕ=0.75 for (c) Shear strength; ϕ=0.75 for (d) Bearing strength; and ϕ=0.7 for (e) Slip resistance)

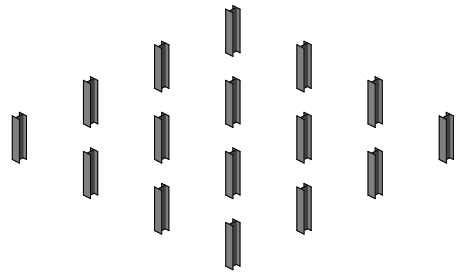

(a) Case 1: One-directional linear arrangement of H-section

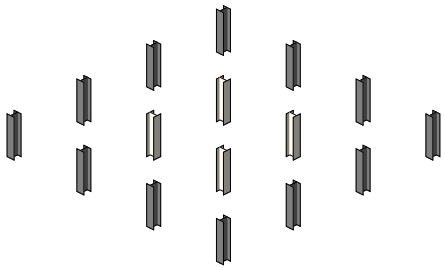

(b) Case 2: Central cross arrangement of H-section

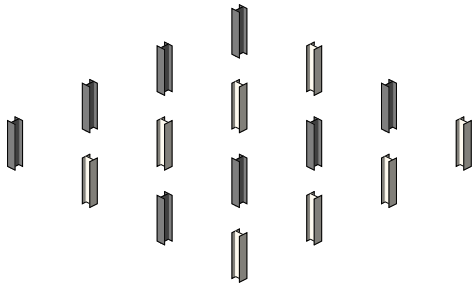

(c) Case 3: Alternating H-section arrangement in each row

Fig. 11 Three types of H-section arrangement for water tank

The bearing strength of the bolt hole was calculated using Eq. (7), with ϕ =0.75, and the slip resistance of the friction connection was determined using Eq. (8), with ϕ=0.7. Both values were confirmed to resist the maximum shear force (R_u). The comprehensive mechanism for each case is illustrated in Fig. 9(b).

$$\phi R_n = \phi \times 1.2 \times L_c \times t \times F_u \quad (7)$$

$$\phi R_n = \phi \times \mu \times h_f \times T_0 \times N_s \quad (8)$$

Where, L_c is the edge distance of a bolt, mm or in.; t is the thickness of the splice plate, mm or in.; F_u is the tensile strength of steel (SS275 grade), MPa or psi; μ is the slip coefficient of the connection; h_f is the bearing factor of the faying surface; T_0 is the design pretension force of high-tension bolts, N or lb; and N_s is the number of shear planes.

All numerical results from this structural verification are visually presented in Fig. 10. The most prominently indicated black bars represent the calculated strength of the specimens, while the solid red line denotes the required strength considering a 70% safety factor, and the red dashed line represents the required strength corresponding to the actual load applied to the water tank. In the strong axis direction, the tensile strength of the high-tension bolts and the out-of-plane bending strength of the splice plates satisfied the design load conditions. Similarly, in the weak axis direction, confirmed to be safe. All joints exhibited stable behavior under the maximum intended load (horizontal shear force of 7 kN and bending moment of 3.5 kN-m).

3. Application to water tank foundation

3.1 Objective

To derive the optimal arrangement/orientation of the developed connections for efficient application in the water tank design, a 3D finite element analysis was conducted. As shown in Fig. 11, three different arrangements of dry connections were evaluated. Case 1 involved H-section connections installed only in one direction. Case 2 involved opposite H-section arrangements at the central region only. Case 3 featured alternating rows of strong and weak axis arrangements of H-section.

The structural analysis model, a 3×3 m (10×10 ft) span

Table 5 Tank design loads

Category		Type	Load values
Gravity load	Dead load	Floor hydrostatic pressure	9.81 kN/m^3×3.4 m=33.4 kN/m^2
	Self weight	SS275	Wall 30 mm, Slab/Roof 10 mm (76.98 kN/m^3)
	Live load	Roof load	1.00 kN/m^2
Lateral load	Seismic load	Centroid action	Per KDS 41 17 00:2022
	Fluid pressure	Wall hydrostatic pressure	9.81 kN/m^3×3.4 m=33.4 kN/m^2

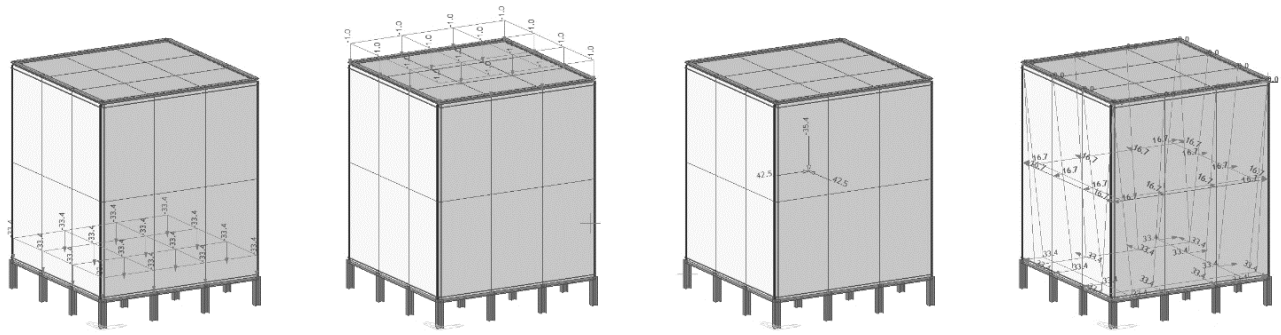

(a) Floor hydrostatic load (DL) (b) Live load (LL) (c) Seismic load (d) Wall hydrostatic load (FP)

Fig. 12 Types of design loads for water tank

tank structure and was implemented using MIDAS Gen to identify member forces acting on the dry pads under seismic loads. The x direction of the seismic load was expressed as E_x and the y direction as E_y. These directions correspond to the previously mentioned strong axis and weak axis directions, respectively.

3.2 Design loads

Seismic loads acting on the water tank were calculated according to KDS 41 17 00: 2022. These loads were classified into horizontal design seismic force and vertical design seismic force, both of which were assumed to act at the center of mass of the tank. Additionally, the hydrostatic pressure due to the water inside the tank was considered as a fixed load acting simultaneously with the seismic load. The structural safety of the connections was evaluated under the most unfavorable load combinations.

3.3 Design seismic load calculation

The total design load of the tank is presented in Table 5, with the application of the design load depicted in Fig. 12. Using the tank weight, which includes dead load and stored water load, the horizontal design seismic force was calculated using Eq. (9)-(11). Vertical design seismic force was determined using Eq. (12). Seismic load coefficients applied in the calculations are provided in Table 6.

$$F_P = \frac{0.4 \times a_p \times S_{DS} \times W_p}{\left(\frac{R_p}{I_p}\right)} \left(1 + 2\frac{z}{h}\right) \tag{9}$$

$$F_{p,\max} = 1.6 \times S_{DS} \times I_p \times W_p \tag{10}$$

Table 6 Specifications of high-tension bolts

Seismic zone	I
Seismic zone coefficient (Z)	0.11g
Return period	2,400
Risk coefficient (I)	2.0
Effective horizontal ground acceleration (S)	0.176
Soil type	S4
Short-period site amplification factor (F_a)	1.448
1 sec-period site amplification factor (F_y)	2.048
Short-period design spectrum acceleration (S_{DS})	0.425
1 sec-period design spectrum acceleration (S_{D1})	0.240
Response modification coefficient (R_p)	2.5
Importance factor (I_p)	1.5

$$F_{p,\min} = 0.3 \times S_{DS} \times I_p \times W_p \tag{11}$$

$$F_p = 0.2 \times S_{DS} \times W_p \tag{12}$$

Where, F_p is the horizontal design seismic force acting at the center of mass of a non-structural element, N or lb; a_p is the amplification factor for the non-structural element; S_{DS} is the design spectral acceleration for short periods; W_p is the weight of the water tank, N or lb; R_p is the response modification factor for the non-structural element; I_p is the importance factor for the non-structural element; z is the height of the attachment point of the non-structural element above the base of the structure, mm or in.; h is the mean roof height of the structure above the base, mm or in.; $F_{p,max}$ is the maximum horizontal design seismic force, N or lb; and $F_{p,min}$ is the minimum horizontal design seismic force, N or lb.

Table 7 Specifications of high-tension bolts

Case	Mode	X		Y		Z	
		Mass (%)	Sum (%)	Mass (%)	Sum (%)	Mass (%)	Sum (%)
1	1	0	0	99.99	99.99	0	0
	2	0	0	0	99.99	99.99	99.99
	3	99.99	99.99	0	99.99	0	99.99
2	1	0.00	0.00	99.76	99.76	0.23	0.23
	2	43.80	43.80	0.14	99.90	56.06	56.29
	3	56.19	99.99	0.091	99.99	43.71	99.99
3	1	78.89	78.86	0	0	21.11	21.11
	2	0	78.86	99.99	99.99	0	21.11
	3	21.11	99.99	0	99.99	78.89	99.99

Table 8 Story forces

Load case	Story	Weight (kN)	Elevation (m)	Seismic force (kN)	Story shear (kN)	Overturning moment (kN-m)
x	Roof	56.396	3.9	58.345	0	0
	2F	359.280	0.5	47.653	58.345	198.372
	1F	0	0	-	105.997	251.370
y	Roof	56.396	3.9	58.345	0	0
	2F	359.280	0.5	47.653	58.345	198.372
	1F	0	0	-	105.997	251.370

3.4 Analysis results

3.4.1 Modal analysis results

Modal analysis for each case was conducted to investigate the dynamic behavior of the structure and establish foundational data for equivalent static analysis. The first mode natural frequency, representing the primary dynamic behavior of the structure, was used in the analysis. Table 7 demonstrates significant variations in modal directions and mass participation ratios across different cases. In Case 1, the mass is primarily concentrated in the *y* direction for Mode 1 (99.99%), while Mode 3 exhibits a complete shift of mass to the *y* direction (99.99%). Conversely, in Case 2, mass participation is more distributed across all three directions, with Mode 1 dominated by the *y* direction (99.76%), while Modes 2 and 3 show increasing mass participation in the *x* direction (43.80% and 56.19%, respectively). Case 3 further emphasizes these directional differences, where Mode 1 shows a dominant contribution in the *x* direction (78.89%), while Mode 2 shifts almost entirely to the *y* direction (99.99%) and Mode 3 is primarily governed by the *z* direction (78.89%). These variations highlight the significant influence of modal shapes on the dynamic behavior of the structure, emphasizing the importance of considering mode- specific mass participation ratios for accurate structural analysis and seismic design.

3.4.2 Seismic analysis results

The strength of a single column was evaluated against the maximum base shear force obtained from the equivalent static analysis (ESA). The ESA is a seismic analysis method primarily used for low-rise buildings, as prescribed in the KDS 41 17 00. This method calculates design seismic loads by substituting them with equivalent static loads proportional to the structure's weight.

Story forces were calculated based on the building weight, as shown in Table 8. The ground surface where the connection is in contact was referred to as the first floor, the area where the water tank is placed was referred to as the second floor, and the topmost part of the water tank was referred to as the roof. The horizontal design seismic force was determined to be 106 kN (24 kips), which is less than the total strength of the 16 columns calculated as 192 kN (43 kips). This indicates that the columns satisfy the seismic strength requirements for typical low-rise buildings. Consequently, they also meet the more stringent seismic strength requirements for non-structural elements.

Using these values, the drift and drift ratio for the *x* and *y* directions were calculated and are illustrated in Fig. 13. A comparison of the two figures shows that in the *x* direction, all cases exhibit relatively uniform and small drift values and drift ratios. This indicates that the structure responds evenly in the *x* direction due to the strong axis arrangement, with member stiffness and design elements effectively resisting *x* axis loads. In contrast, in the *y* direction, Case 1 shows a significant increase in first-story drift compared to the other cases. This suggests that the structural design in Case 1 might not provide sufficient stiffness or damping in the first story for *y* direction loads. Additionally, the second story exhibits minimal drift in the *y* direction, indicating that *y* axis loads are primarily concentrated on the first story.

In conclusion, alternating arrangement of the strong and

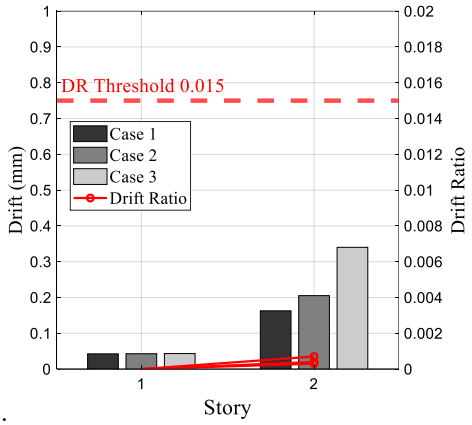

(a) Comparison in x direction

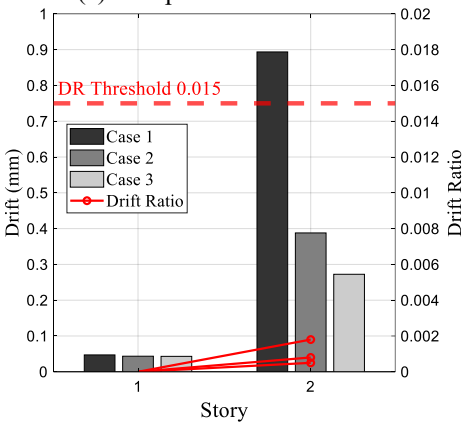

(b) Weak axis y direction

Fig. 13 Maximum story drift

weak axes allows for effective resistance to lateral loads along both the x and y axes. However, as all drift ratios are below the safety limit of 0.015, Case 1 can still be considered a viable arrangement when considering constructability. Nevertheless, it is advisable to further review reinforcement measures for the first floor, considering the displacement in the y direction. Future studies should incorporate nonlinear analysis to examine structural behavior more precisely and include additional evaluations reflecting various ground conditions and loading scenarios.

4. Conclusions

This study experimentally evaluated the structural performance of H-section steel dry connections for tank foundations and conducted analyses to derive the optimal arrangement. The main findings of the study are as follows:

1) The static lateral force tests for the strong and weak axes of H-section revealed that deformations in all specimens were concentrated at the lower joint rather than the column body. In the strong axis direction, specimens with sequential bolt slippage exhibited higher yield strength, whereas the opposite trend was observed in the weak axis direction. This was attributed to differences in stress distribution depending on the loading direction.

2) The strength evaluation of the joints confirmed that the proposed height-adjustable connections satisfy the intended load conditions (horizontal shear force of 10 kN, bending moment of 3.5 kN-m). Specifically, the tensile strength of high-tension bolts and the out-of-plane bending strength of splice plates in the strong axis direction, as well as the shear strength of high-tension bolts and the bearing strength of bolt holes in the weak axis direction, met the requirements.

3) Structural tests on individual dry columns demonstrated a minimum strength of 10 kN (2.2 kips) both for the strong and weak axes. This indicates that the total strength of the 16 dry connections is sufficient to resist not only the horizontal design seismic force for non-structural components but also the more stringent criteria for low-rise buildings.

4) The 3D finite element analysis using MIDAS showed that all arrangement cases (Cases 1, 2, and 3) satisfied the story drift and stability coefficient criteria. Therefore, considering constructability, Case 1, which arranges the dry connections in the same direction, is proposed as the optimal configuration.

5) The proposed height-adjustable dry connection system overcomes the limitations of conventional concrete wet connections while ensuring sufficient structural performance. In particular, the height adjustment feature significantly enhances constructability and maintenance efficiency.

The results of this study present an innovative improvement for water tank foundation systems and are expected to serve as a practical alternative in the field of water resource infrastructure construction in the future.

Acknowledgments

This research was supported by National Research Foundation of Korea (No. 2021R1A5A1032433), by Sookwang Tech, and by the Institute of Construction and Environmental Engineering at Seoul National University. This work was also supported by the Institute of Information & Communications Technology Planning & Evaluation (IITP) grant and KoFONS grant funded by the Korean government (MSIT and NSSC) (No. 2021-0-01343 and 220324), respectively.

References

American Concrete Institute (2006), Seismic Design of Liquid-Containing Concrete Structures and Commentary (ACI350.3-06), American Concrete Institute, Farmington Hills, MI, USA.

American Society of Civil Engineers (2017), ACE/SEI 7-16: Minimum Design Loads and Associated Criteria for Buildings and Other Structures, American Society of Civil Engineers, Reston, VA, USA.

American Water Works Association (2011), ANSI/AWWA D100-11: Welded Carbon Steel Tanks for Water Storage, American Water Works Association, Denver, CO, USA.

Baek, J. and Choi, Y. (2017), "Review of the seismic design method of water tanks for buildings", *Proc. Autumn Conf. Arch. Inst. Korea*, **37**(2), 68-75.

Baek, J., Kim, S. and Choi, Y. (2019), "Evaluation of seismic design force by earthquake response analysis of water tanks installed in RC buildings", *EESK J. Earthq. Eng.*, **23**(4), 221-229. https://doi.org/10.5000/EESK.2019.23.4.221.

Brunesi, E., Nascimbene, R., Pagani, M. and Beilic, D. (2015), "Seismic performance of storage steel tanks", *Earthq.*, **29**, 503-510. https://doi.org/10.1061/(ASCE)CF.1943-5509.0000628.

Cruz, E.F. and Valdivia, D. (2011), "Performance of industrial facilities in the Chilean earthquake of 27 February 2010", *Struct. Des. Tall Spec. Build.*, **20**, 83-101. https://doi.org/10.1002/tal.679.

Fasaee, M.A.K., Banan, M.R. and Ghazizadeh, S. (2018), "Capacity of exposed column base connections subjected to uniaxial and biaxial bending moments", *J. Constr. Steel Res.*, **148**, 361-370. https://doi.org/10.1016/j.jcsr.2018.05.025.

Fischer, E.C., Liu, J. and Varma, A.H. (2016), "Investigation of cylindrical steel tank damage at wineries during earthquakes: Lessons learned and mitigation opportunities", *Prac. Period. Struct. Des. Constr.*, **21**, 1301-1328. https://doi.org/10.1061/(ASCE)SC.1943-5576.0000283.

Hosseini, S.E.A. and Beskhyroun, S. (2023), "Fluid storage tanks: A review on dynamic behaviour modelling, seismic energy-dissipating devices, structural control, and structural health monitoring techniques", *Struct.*, **49**, 537-556. https://doi.org/10.1016/j.istruc.2023.01.146.

Hou, H., Wang, C., Qu, B. and Liang, Y. (2021), "Cyclic testing of bolted base connections for wide-flange columns", *Eng. Struct.*, **235**, 1-11. https://doi.org/10.1016/j.engstruct.2021.112024.

Housner, G.W. (1957), "Dynamic pressures on accelerated fluid containers", *Bull. Seismol. Soc. Am.*, **47**(1), 15-35. https://doi.org/10.1785/BSSA0470010015.

Japan Architecture Center (2014), Recommendation for Seismic Design and Construction of Building Equipment, Japan Architecture Center, Tokyo, Japan.

Kanvinde, A.M., Jordan, S.J. and Cooke, R.J. (2013), "Exposed column base plate connections in moment frames — Simulations and behavioral insights", *J. Constr. Steel Res.*, **84**, 82-93. https://doi.org/10.1016/j.jcsr.2013.02.015.

KDS 14 31 25:2017 (2017), Design Standards for Steel Structure Connections - Load and Resistance Factor Design, Seoul, Korea.

KDS 17 10 00:2018 (2018), General Guidelines for Seismic Design, Korean Society of Steel Construction, Seoul, Korea.

KDS 41 00 00:2022 (2022), Structural Design Standards for Buildings, Korean Society of Steel Construction, Seoul, Korea.

KDS 41 17 00:2019 (2019), Seismic Design Standards for Buildings, Korean Society of Steel Construction, Seoul, Korea.

KDS 41 31:2019 (2019), Design Standards for Steel Structures in Buildings, Korean Society of Steel Construction, Seoul, Korea.

Khosravi, J. and Daire, A.B. (2019), "External cathodic protection of concrete-pad mounted aboveground storage tank: Necessity or choice?", *NACE Corrosion 2013*, Orlando, FL, USA, March.

Kim, H.S., Oh, J. and Jung, H.Y. (2016), "Shaking table test of a stainless water tank with natural rubber bearing", *J. Korea Acad. Industr. Cooper. Soc.*, **17**(44), 52-58. https://doi.org/10.5762/KAIS.2016.17.4.52.

Kong, Z., Hu, N., Jin, Y., Xing, K., Tai, Q., Vasdravellis, G., Thai, D.K. and Vu, Q.V. (2024), "Shear capacity of additive-manufactured stainless-steel single-lap bolted connections", *Steel Compos. Struct.*, **53**(2), 227-241. https://doi.org/10.12989/scs.2024.53.2.227.

KS D 3503:2018 (2018), Rolled Steels for General Structure, Korean Standards Association, Seoul, Korea.

Lee, S.E. and Lee, D.M. (2023), "Development of numerical modelling techniques for a firefighting water tank with an anti-wave plate under seismic loads", *Appl. Sci.*, **13**(11), 1-15. https://doi.org/10.3390/app132111689.

Lim, W.Y., Lee, D. and You, Y.C. (2017), "Exposed column-base plate strong-axis connections for small-size steel construction", *J. Constr. Steel Res.*, **137**, 286-296. https://doi.org/10.1016/j.jcsr.2017.06.018.

Liu, X.C., Cui, F.Y., Zhan, X.X., Yu, C. and Jiang, Z.Q. (2019), "Seismic performance of bolted connection of H-beam to HSS-column with web end-plate", *J. Constr. Steel Res.*, **156**, 167-181. https://doi.org/10.1016/j.jcsr.2019.01.024.

Nechache, A. and Bouzid, A. H. (2007), "Creep analysis of bolted flange joints", *Int. J. Press. Vessel. Pip.*, **84**, 185-194. https://doi.org/10.1016/j.ijpvp.2006.06.004.

Park, S., Won, S., Choi, M., Kim, S. and Cheung, J. (2013), "Seismic performance evaluation of externally reinforced panel water tank using shaking table tests", *EESK J. Earthq. Eng.*, **17**(4), 151-157. https://doi.org/10.5000/EESK.2013.17.4.151.

Praveen, K.M., Thomas, W. and Martin, W. (2000), "Simple procedure for seismic analysis of liquid-storage tanks", *Struct. Eng. Int.*, **197**(5), 1-5. https://doi.org/10.2749/101686600780481509.

Robert, D. (1964), "Controlled water test to preload tank foundations", *J. Soil Mech. Found. Div.*, **90**, 5-15. https://doi.org/10.1061/JSFEAQ.0000657.

Sobhan, M.S., Rofooei, F.R. and Attari, N.K.A. (2017), "Buckling behavior of the anchored steel tanks under horizontal and vertical ground motions using static pushover and incremental dynamic analyses", *Thin Wall. Struct.*, **112**, 173-183. https://doi.org/10.1016/j.tws.2016.12.022.

Stewart, J.P., Fenves, G.L. and Seed, R.B. (1999), "Seismic soil-structure interaction in buildings. I: Analytical methods", *J. Geotech. Geoenviron. Eng.*, **125**, 26-37. https://doi.org/10.1061/(ASCE)1090-0241(1999)125:1(26).

Thakur, A., Jain, A. and Rathore, R. (2017), "Seismic analysis of elevated water tank with variations of H/D ratio and container shape using STAAD-Pro V8i", *Int. J. Trend Res. Dev.*, **4**(5), 1-6.

Torres-Rodas, P., Zareian, F. and Kanvinde, A. (2018), "A hysteretic model for the rotational response of embedded column base connections", *Soil Dyn. Earthq. Eng.*, **115**, 55-65. https://doi.org/10.1016/j.soildyn.2018.08.015.

Ulloa-Rojas, J., Colombo, J., Wilches, J., León, R. and Almazán, J. (2024), "Influence of soil-foundation-tank interaction on buckling strength of liquid storage tanks", *Eng. Struct.*, **305**, 1-15. https://doi.org/10.1016/j.engstruct.2024.117744.

Ximei, Z., Haosong, W. and Feng, F., "Multi-physics coupling method and applications of fluid-structure interaction on LNG storage tanks", *11th World Congress on Computational Mechanics (WCCM XI)*, Barcelona, Spain, July.

Yazdanian, M., Ingham, J.M., Kahanek, C. and Dizhur, D. (2020), "Damage to flat-based wine storage tanks in the 2013 and 2016 New Zealand earthquakes", *J. Constr. Steel Res.*, **168**, 1-11. https://doi.org/10.1016/j.jcsr.2020.105983.

Zareian, F., Sampere, C., Sandoval, V., McCormick, D.L., Moehle, J. and Leon, R. (2012), "Reconnaissance of the Chilean wine industry affected by the 2010 Chile offshore Maule earthquake", *Earthq. Spectra*, **28**, 503-512. https://doi.org/10.1193/1.4000048.

DL